Slow Fluorescence from Perturbed Glyoxal (S_1) Levels Observed under Collision-Free Conditions

J. Heldt,† Ch. Ottinger,* A. F. Vilesov, and T. Winkler

Max-Planck-Institut für Strömungsforschung, Bunsenstrasse 10, D-37073 Göttingen, Federal Republic of Germany

Received: August 8, 1996; In Final Form: October 14, 1996[⊗]

Jet-cooled *trans*-glyoxal molecules were excited in the $^1S_1 \leftarrow {}^1S_0$ transition using a pulsed, narrow-band (0.10-cm^{-1}) dye laser. Collision-free conditions were ensured using a large nozzle−laser beam distance (27 mm) and low stagnation pressures (∼80 Torr). Spectrally unresolved fluorescence was observed with a photomultiplier viewing either the excitation region itself or a region of the molecular beam well downstream (46 mm) from the laser beam. Respectively, detection time windows of 0−6 and 30−80 μs after the laser pulse were used. In the latter case, the signal intensity was $\sim 2 \times 10^{-3}$ of the former. This is at least 100 times greater than calculated from the known S_1 glyoxal fluorescence lifetime (2.4 μs). However, only certain isolated rovibronic levels exhibit this anomalously slow fluorescence. The rotationally resolved excitation spectra of 17 $S_1 \leftarrow S_0$ bands were recorded both in the "slow" and "prompt" fluorescence mode. While the latter showed the usual dense line pattern, the former consisted of much fewer distinct lines, their number increasing with the excess vibrational energy. The corresponding emitting levels owe their long lifetime to the partial triplet character of their wave function, due to accidental resonance with T_1-state levels. For the 0_0^0 and 5_0^1 $S_1 \leftarrow S_0$ bands, the rotational quantum numbers of the perturbed S_1 levels were determined from a computer simulation. This is the first state-specific, collision-free observation of the previously predicted fluorescence lifetime lengthening through intramolecular S_1/T_1 coupling in small organic molecules. It could, in fact, be shown experimentally that in previous reports on the glyoxal phosphorescence excited in the S_1 region, collisional effects must have obscured the behavior of the isolated molecules.

1. Introduction

The coupling of the excited singlet and triplet states of small molecules has been a subject of interest for many years (refs 1−3 and references therein). An especially prominent manifestation of this coupling is the quenching of singlet fluorescence, induced by collisional transitions into the triplet state. Glyoxal is a convenient molecule for these studies, because the excitation energies of the first excited singlet and triplet states S_1 and T_1 both lie in the visible region of the spectrum, at 455 and 521 nm, respectively.[4] This molecule thus has a relatively small singlet−triplet energy gap of ∼2800 cm^{-1}, and consequently, the density of the T_1 vibrational levels in the region of the vibrationless S_1 state is low. For this reason, glyoxal has served for decades as a prototype of a so-called intermediate case species, defined as having a natural level width comparable to the average level spacing.[2]

In order to describe the observed intersystem crossing effects in small polyatomic molecules, the so-called "gateway" theory was developed.[5,6] According to this mechanism, a few isolated rotational levels of the S_1 state are perturbed by S/O interaction with accidentally resonant T_1 levels. These levels serve as so-called gateways in the collision-induced energy transfer from S_1 to T_1. In glyoxal, state mixing between singlet and triplet rotational levels has been observed under application of a strong magnetic field.[7] Perturbations in the absence of an external field can in principle be observed by means of high-resolution spectroscopy (see, e.g., ref 8 for the case of pyrimidine). For the glyoxal $S_1 \leftarrow S_0$ transition, however, high-resolution spectra of vibronic bands[9−11] have given no indication of any S_1/T_1 perturbations on the basis of line shifts.

Collision-induced intersystem crossing (ISC) $S_1 \rightarrow T_1$ in glyoxal was studied as early as 1971 by Parmenter's laboratory,[12] using Hg atomic line and flash excitation. In a later work by the same group, the crossing mechanism was discussed in terms of the wavefunction mixing between the "singlet" and "triplet" levels.[13] Subsequently, Lineberger and co-workers made a comprehensive study of collisional S_1 glyoxal quenching,[14,15] using pulsed laser excitation and time-resolved fluorescence detection. Again ISC from the ^1A_u (S_1) to the ^3A_u (T_1) state was shown to be the principal singlet quench mechanism, through direct observation of the long-lived $T_1 \rightarrow S_0$ phosphorescence.[15] For the particular case of 0_0^0 excitation, Michel et al. were able to identify well-specified, isolated gateway levels and to demonstrate the role which they play in the collision-induced intersystem crossing (CI ISC) in glyoxal.[16] Steric effects of the collisional S_1/T_1 coupling in glyoxal have also been studied[17] by means of excitation of specific isomeric $C_2H_2O_2$−Ar van der Waals complexes and time-resolved measurements of their dephasing rate constants.

On the other hand, the possibility of collision-free $S_1 \rightarrow T_1$ transitions in glyoxal has received much attention in the past. In a similar molecule, biacetyl, such intramolecular processes had been observed in an early work.[18] In glyoxal, however, a search at a qualitative level[15] showed no delayed, i.e., phosphorescence, emission at very low pressures (<1 mTorr), neither with excitation near the S_1 origin nor at higher energy, e.g., at the ν_8 (b_g) mode. Thus the production of the ^3A_u state from the ^1A_u state was ascribed exclusively to "external perturbations", i.e., collisions. Two further investigations[19,20] also arrived at the conclusion that in glyoxal $S_1 \rightarrow T_1$, ISC does not occur in the absence of collisions (at least not in the ordinary $(CHO)_2$ molecule; concerning $(CDO)_2$, the two studies disagreed). Both groups found that after laser excitation of the S_1

† On leave from the University of Gdańsk, 80-952 Gdańsk, Poland.

⊗ Abstract published in *Advance ACS Abstracts,* December 15, 1996.

S1089-5639(96)02422-X CCC: $14.00

state, the phosphorescence yield was zero in the low-pressure limit. Indeed, in ref 20, a special effort was made to search for the expected slow emission component from coupled S_1/T_1 levels. An upper limit of the fluorescence intensity ratio $I_{slow}/I_{prompt} \leq 5 \times 10^{-3}$ was estimated in this particular experiment.

In 1980, Jouvet and Soep employed for the first time excitation of glyoxal in a pulsed jet instead of a cell.[21] This enabled them to prepare the S_1 state of this molecule selectively in specified rovibronic levels. Fluorescence and phosphorescence excitation spectra were recorded. For the former, emission was observed from the Mach bottle zone, i.e., under practically collision-free conditions. Phosphorescence was observed from the Mach disk region, where the flow velocity is reduced sufficiently for long-lived emission to become observable. It was the premise of this work that the T_1 state is populated entirely by collisions from the laser-excited S_1 state, as concluded by Lineberger et al.[15] Large cross sections (σ_{ISC}) were derived. The two types of excitation spectra were found to be generally quite similar. This indicated the presence of multiple collisions, since the gateway theory of collisional ISC predicts a cross section proportional to the T_1 content of the S_1 wave function, which should vary erratically from one S_1 rovibronic level to another. In one case, however, anomalously intense spikes in the phosphorescence spectrum gave evidence of an accidental resonance and therefore exceptionally efficient S_1/T_1 coupling.

In 1984, the introduction of the "sensitized phosphorescence" technique by Ito and his group[22] opened a novel way to efficient detection of long-lived T_1 state molecules. In ref 23, a test experiment done with biacetyl showed that the yields of the sensitized (surface-induced) phosphorescence and of the phosphorescence emission in free flight (up to 40 μs after the excitation) are very closely proportional to each other. This observation established the sensitized phosphorescence technique as a convenient and reliable means of monitoring the population of the T_1 state following S_1 excitation, be it by collisional $S_1 \rightarrow T_1$ transfer or otherwise. For glyoxal and two related molecules, the branching between $S_1 \rightarrow T_1$ transfer and $S_1 \rightarrow S_0$ fluorescence emission was then obtained from a comparison of the sensitized phosphorescence and fluorescence excitation spectra. These spectra differed greatly in the relative band intensities, indicating a distinct vibrational mode selectivity of the ISC process. For example, the out-of-plane vibrations of glyoxal were found to strongly promote the $S_1 \rightarrow T_1$ transfer. However, the question of the ISC mechanism, i.e., whether it is collision-induced or intramolecular, was not explicitly addressed in this paper.

In subsequent work on glyoxal by the same group,[24] this point was taken up expressly. Here, similar to ref 21, rotationally resolved fluorescence and phosphorescence excitation spectra were compared, the main experimental difference being that now for the latter the sensitized phosphorescence detection was used. Apart from an unexplained intensity alternation with the nuclear spin symmetry of the excited rovibronic level, the two types of spectra across a given band were found to be quite similar, in agreement with ref 21. Contrary to ref 21, however, it was argued here that the intersystem crossing occurred more or less intramolecularly. To support this claim, fluorescence lifetime measurements were made, which gave results ($\tau = 2.4$ μs) identical with the extrapolated zero-pressure lifetime from Lineberger's work.[14]

However, Jouvet and Soep[21] also obtained this same lifetime of 2.4 μs in their apparatus, yet they assumed that the $S_1 \rightarrow T_1$ process was exclusively collisional. Clearly the important question of what really causes the $S_1 \rightarrow T_1$ transfer in glyoxal requires further study. In neither of the two controversial papers[21,24] are the beam conditions such that collisional effects could have been discarded a priori. The present work gives the first unambiguous proof of S_1/T_1 coupling in glyoxal under strictly collision-free conditions, such as was unsuccessfully searched for in refs 15, 19, and 20. Moreover, it could be shown that the $S_1 \rightarrow T_1$ transfer observed in ref 24 must actually have been collision-dominated, as it was in ref 21. We were able to vary the pressure conditions such that we could trace the transition from the collision-controlled to the truly intramolecular domain. Scanning the laser across a given band of the glyoxal $S_1 \leftarrow S_0$ transition as in refs 21 and 24, rotationally resolved excitation spectra were recorded for two detection time windows: (a) using a detection gate of 6 μs following immediately after the laser pulse or (b) integrating the emission over the interval $\Delta t = 30-80$ μs. At high pressures at the excitation region, the two excitation spectra were quite similar. This parallels the results of refs 21 and 24. However, increasing the nozzle−laser beam distance up to $x = 27$ mm, the "delayed emission" excitation spectrum, b, differed greatly from the usual fluorescence spectrum, a. It was generally sparser than spectrum a and for some bands consisted of only very few lines. The delayed emission, under strictly collision-free excitation conditions, is due to those S_1 rovibronic levels which are intramolecularly perturbed by accidental near-resonance with T_1 levels. The attendant fractional triplet character in the wave functions lengthens the lifetimes of these isolated S_1 levels to such an extent that their emission can be detected under condition b. In agreement with the usage of ref 20, we call this emission "slow fluorescence" rather than phosphorescence, since a fairly moderate admixture of triplet character is sufficient for observation in the delayed time window, given sufficient detection sensitivity. In the present work, the type b spectra were about 500 times weaker than the ordinary, prompt fluorescence spectra, a, which explains why no slow fluorescence was seen in ref 20 with an estimated sensitivity limit of 5×10^{-3}. The term "phosphorescence excitation" used in the previous studies (e.g., refs 19−24) describes, as we now know, a collision-dominated $S_1 \rightarrow T_1$ transfer. By contrast, the label "slow fluorescence" is intended to emphasize that we are observing emission directly from the laser-excited S_1 level as in any fluorescence, except that this particular level is perturbed. The slow fluorescence excitation spectra thus map out the intramolecular gateways between the S_1 and T_1 manifolds of glyoxal. For the $S_1 \leftarrow S_0$ 0_0^0 and 5_0^1 bands, they could be precisely identified by means of computer simulation of the spectra. This then establishes a firm basis for the much discussed gateway-type collisional quenching of the S_1 state of glyoxal.

2. Experimental Section

trans-Glyoxal was prepared by a similar procedure as described in an earlier work.[25] A mixture of glyoxal trimer dihydrate and P_2O_5 (both obtained from Aldrich) was heated under vacuum. This is known to release glyoxal in the form of the monomer, which was passed through a stainless steel liquid nitrogen trap in which the glyoxal molecules condensed. Any remaining gas, such as glyoxal decomposition products, was removed by a mechanical vacuum pump. For further purification, the glyoxal sample accumulated in the cold reservoir was sealed off from the source container and from the pump, allowed to warm to room temperature, and cooled again to liquid nitrogen temperature, and any noncondensable gases were again pumped off. This cycle was gone through several times, as an extra precaution against impurities. The

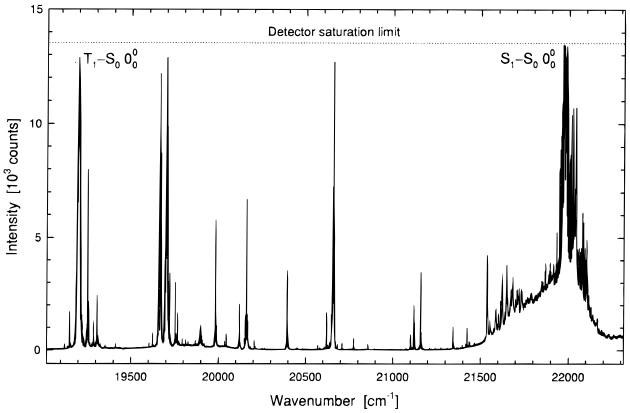

Figure 1. Overview excitation spectrum of the laser-induced long-lived emission from jet-cooled *trans*-glyoxal molecules. The photomultiplier tube here was positioned 69 mm downstream from the laser excitation region. Seed ratio 7 Torr of glyoxal in 145 Torr of H_2. Laser pulse repetition rate 30 Hz, scan rate 0.02 Å/s. The SSR photon counter saturates at about 10 MHz. With the time window of 40 μs used here (from 35 to 75 μs after the laser pulse), this corresponds to an expected saturation limit of 12 000 counts per readout interval of 1 s. The observed saturation limit is 13500 counts. From the $T_1 \leftarrow S_0$ origin at 19 200 cm^{-1} (corresponding to 521 nm) up to ~21 500 cm^{-1} (465 nm), the spectrum shows the laser-induced phosphorescence (LIP) emitted from T_1 levels. Surprisingly, intense long-lived emission is also observed near the $S_1 \leftarrow S_0$ origin, on the right. It is due to S_1 levels having partial T_1 character and thereby emitting slow fluorescence. The quasi-continuum underlying the $S_1 \leftarrow S_0$ 0_0^0 band (here greatly exaggerated, due to saturation of the peak intensity) is not understood. It includes $S_1 \leftarrow S_0$ hot bands but appears to contain other contributions, possibly from glyoxal dimers. *cis*-Glyoxal, whose $S_1 \leftarrow S_0$ 0_0^0 band would appear at 20 500 cm^{-1},[28] can be seen to be absent in the sample used.

sample was stored for up to 2 weeks, substituting the liquid nitrogen by thermoelectric cooling using a photomultiplier tube housing (Products for Research, Model TE 104). This provides a stable temperature of ~ −30 °C (manufacturer's data). Under these conditions, the glyoxal vapor pressure was 10−12 Torr, suitable for the experiments.

The molecular beam/laser arrangement used in this work has been described in detail in our earlier work on pyrimidine.[26,27] The glyoxal vapor from the reservoir at ~10 Torr was seeded in ~70 Torr of Ar and expanded through a pulsed nozzle (1-mm diameter, pulse length 250 μs, repetition rate 10 or 30 Hz). Downstream from the nozzle (27 mm), the glyoxal molecules were excited by an excimer-pumped dye laser beam (Lambda Physik, EMG 202 MSC and FL 3002 E). In some cases, a distance of 7 mm between nozzle and excitation zone was used. The laser was operated with the dyes coumarine 2 and coumarine 102, providing pulses in the 415−460-nm wavelength region, synchronized with the nozzle (bandwidth ~0.10 cm^{-1}, pulse energy 1−15 mJ, which was appropriately attenuated to avoid detector saturation). In the measurement of the LIP $T_1 \leftarrow S_0$ excitation spectrum shown in Figure 1, the dyes coumarine 120 and coumarine 307 were used additionally, in order to extend the excitation region up to 525 nm. Undispersed laser-induced emission was observed by a cooled photomultiplier, and excitation spectra were obtained by scanning the laser and storing the photon counts in a multichannel data acquisition system (CMTE-Fast MCD/PC). For the high-resolution spectra shown below (Figures 3−7, 9, and 10), the laser was scanned very slowly (~0.025 cm^{-1}/s), and data were read out at intervals of 1 s.

The photomultiplier tube (EMI 9829 QGA) was placed inside the vacuum chamber complete with its thermoelectric cooler housing (Products for Research, model TE 104) and preamplifier/discriminator (PAR, Model SSR 1120). The tube was positioned such that points on the molecular beam axis either 17 mm or 46 mm downstream from the excitation region were imaged onto the center of the PM photocathode. Imaging optics (1:1) was used, consisting of two 50-mm focal length lenses. No spectral filtering was employed. With the "near" (17-mm) position of the photomultiplier tube, the observation region included the excitation zone, owing to the large (46-mm-diameter) photocathode. In this mode, standard LIF spectra of the $S_1 \leftarrow S_0$ transition were recorded. The "far" (46-mm) position of the PM tube was used to observe the slow fluorescence, which is the essential discovery of this work. The bright, prompt LIF emission from the glyoxal S_1 state, having a lifetime of ≤2.4 μs,[15] is confined to the immediate vicinity of the excitation point (extending ~3 mm downstream). In the far PM position, this "prompt", intense light cannot reach the PM cathode, due to the short emitter lifetime. It is important to shield the detector carefully against stray fluorescence light from the excitation zone. Only light emitted by long-lived species from points lying between 23 and 69 mm downstream from the excitation region will then contribute to the signal. At the calculated molecular beam speed of 560 m/s, this corresponds to a time of flight of between 40 and 120 μs after the laser excitation. Precisely defined detection time windows for the two observation modes were provided by electronic gating of the photon counts. For the near and far positions of the PM tube, the gate was open from 0 to 6 μs and (with empirical optimization) from 30 to 80 μs after the laser pulse, respectively. Since the prompt $S_1 \rightarrow S_0$ fluorescence is very intense, the laser beam was for these measurements attenuated by a factor of 10^{-5}−10^{-8}, using neutral density filters, in order to prevent the photon counter from being saturated. The slow fluorescence is weaker by 3 orders of magnitude. The laser beam here was attenuated by a factor of 10^{-2}−10^{-5}.

3. Results

Figure 1 illustrates qualitatively the experimental finding which led to the present study. In the course of a systematic study of direct laser excitation of the glyoxal T_1 state,[29] the laser frequency was scanned from the onset of phosphorescence, at the $T_1 \leftarrow S_0$ origin, to the region of the $S_1 \leftarrow S_0$ transition. Undispersed emission was detected by a photomultiplier positioned 46 mm downstream from the exciting laser beam so that only the long-lived phosphorescence was observed. This setup is identical to that used by us in measurements of the laser-induced phosphorescence (LIP) excitation spectra of pyrimidine and pyrazine[26] and is a slight variation of the arrangement used earlier by Pratt and co-workers[25,30,31] for similar LIP experiments on glyoxal. With improved detection sensitivity, we observed a very large number of vibrational bands in the T_1 state (see Figure 1, in the region below ~21 500 cm^{-1}). Their detailed analysis is in preparation.[29] The high sensitivity enabled us to follow the T_1 vibrational excitation to much higher levels than was done in ref 30. The average intensity of the bands decreased sharply in going to shorter laser wavelengths—much more than is apparent from Figure 1, since the bands on the left of the figure are strongly saturated. However, contrary to this decreasing trend, strong emission set in again at about $\Delta\tilde{\nu}$ = 2770 cm^{-1} above the $T_1 \leftarrow S_0$ origin, close to the $S_1 \leftarrow S_0$ threshold. It is obviously related to S_1 excitation, although it cannot be the ordinary short-lived (τ = 2.4 μs) fluorescence which does not contribute at the observation point chosen in this particular experiment. This finding represents the first observation of the slow fluorescence in glyoxal, which was previously unsuccessfully searched for by other groups.[15,20] In our experiment, it appears with very large intensity, about 25−

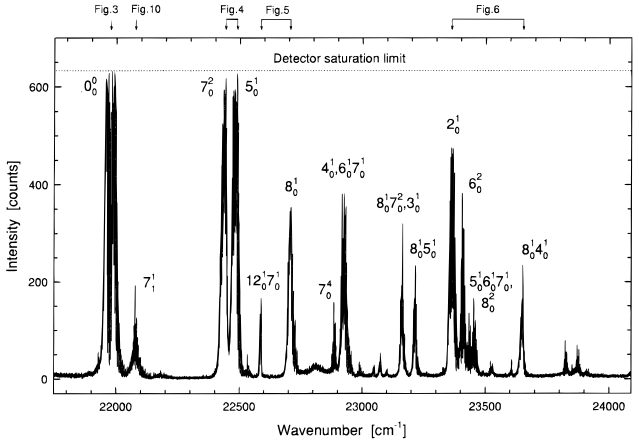

Figure 2. Overview excitation spectrum of the laser-induced short-lived $S_1 \leftarrow S_0$ emission from glyoxal. The photomultiplier tube viewed the excitation zone directly. The 17 bands for which slow and prompt fluorescence was observed at high resolution are labeled. At the top, the bands shown in the respective figures are marked, in order of increasing excess energy over the S_1 origin. The laser repetition rate here was 10 Hz; the observation gate was from 0 to 6 μs after the laser pulse. This corresponds to a saturation limit 25 times less than in Figure 1, which is consistent with the observed relative cutoff (635 vs 13500 counts/s).

200 times that of a typical LIP band (in Figure 1, the region near the $S_1 \leftarrow S_0$ origin is again heavily saturated). We therefore decided to study the long-lived S_1 glyoxal states systematically and with high resolution.

Figure 2 gives an overview of the glyoxal $S_1 \leftarrow S_0$ bands, excited in the usual laser-induced fluorescence (LIF) scheme. Thus, the photomultiplier here was positioned such that it viewed the excitation region directly. Again, most of the bands are heavily saturated. This spectrum is shown here only for general orientation, indicating the location of the specific bands to be discussed below. The identification of the labeled bands follows ref 32.

Figures 3−6 show high-resolution scans of seven selected $S_1 \leftarrow S_0$ bands (out of the 17 bands, labeled in Figure 2, which were studied in this way). The emphasis is in each case on the juxtaposition of the ordinary prompt LIF and the slow LIF excitation spectra, as recorded with the photomultiplier in the near and far positions, respectively (see section 2).

For the 0_0^0 band, Figure 3 gives two such spectra in the top two panels. They were recorded with the nozzle far removed from the laser excitation zone ($x = 27$ mm), in order to ensure truly collision-free flight of the excited molecules up to the detection region. The prompt fluorescence spectrum (b) shows the typical rotational band contour of a perpendicular c-type band (cf. the spectrum simulation, section 4). It agrees well with an $S_1 \leftarrow S_0$ 0_0^0 absorption spectrum reported earlier,[9] except that in the latter case the rotational excitation was that of the room-temperature sample. The central section of Figure 3b can also be compared with the high-resolution fluorescence excitation spectra given in refs 21, Figure 2A, and 24, Figure 1a. In both cases, the overall structure is similar to that shown in Figure 3b, although the rotational temperature was lower in refs 21 and 24 due to the much higher expansion pressures used. Our slow fluorescence spectrum, Figure 3a, is seen to be profoundly different from the ordinary, prompt LIF spectrum, Figure 3b. It is much less dense, and the line pattern appears chaotic compared to the well-ordered groups of lines in the standard LIF spectrum. We attribute this to the presence of a small number of accidental coincidences between isolated S_1 and T_1 rotational levels. S/O coupling mixes some T_1 character

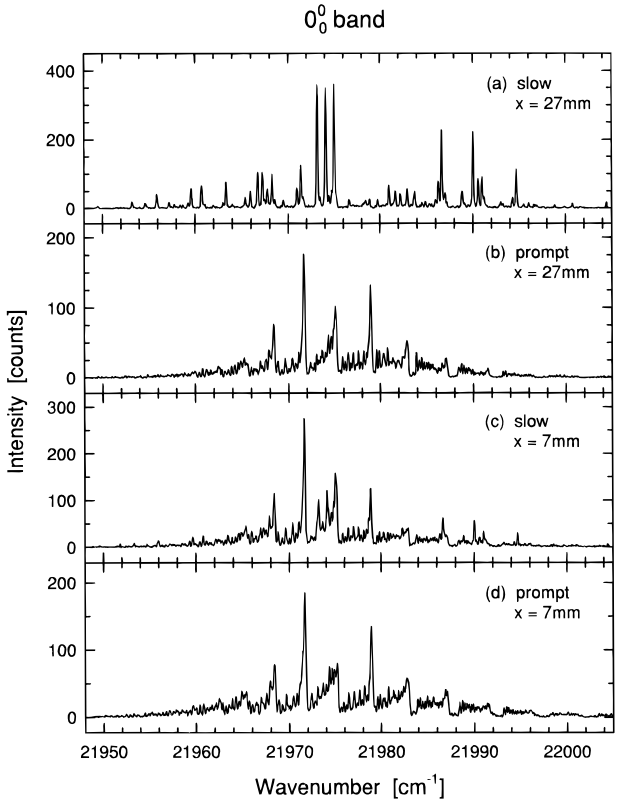

Figure 3. High-resolution excitation spectra of the $S_1 \leftarrow S_0$ origin band 0_0^0 of jet-cooled glyoxal. Seed ratio 12 Torr of glyoxal in 75 Torr of Ar. Laser repetition rate 10 Hz, scan rate 0.006 Å/s. (a) Slow fluorescence, selected by positioning the photomultiplier tube 46 mm downstream from the excitation zone. (b) Prompt (total) fluorescence, as observed viewing the excitation zone directly. (c and d) Slow and prompt LIF excitation spectra as in a and b but for a much shorter nozzle−laser distance x as indicated. Due to the different molecular beam densities, as well as different laser attenuation used for prompt and slow LIF, none of the ordinate scales can be directly compared. An estimate of the intensity ratio of the highest peaks in spectra a and b, from the count rates and the attenuation factors, is b/a $\approx$ 470. Note the complete dissimilarity of spectra a and b, indicating the special intramolecular effects which enable certain lines to appear in the "slow LIF" condition. By contrast, the differences between "slow" and "prompt" LIF are largely eliminated at $x = 7$ mm, panels c and d. Here, collisional effects obscure the intramolecular S_1/T_1 coupling, as was apparently also the case in previous work[21,24] (see text).

into the S_1 wave function and thereby lengthens the lifetime of that particular S_1 level. An "erratic"[21] dependence of this intramolecular coupling on the rovibronic level, such as we are observing, was, in fact, predicted in ref 21 but was not found. Unlike the present work, in both refs 21 and 24, the excitation spectra of the long-lived species closely resembled the common LIF spectra: The phosphorescence excitation spectrum in ref 21, Figure 2B, was found to be "almost identical" to the fluorescence excitation spectrum, Figure 2A, and also in ref 24, there is a great similarity between the (sensitized) phosphorescence and the fluorescence excitation spectrum (Figure 1b vs 1a in ref 24).

As explained in the Introduction, collisional effects could be expected to have played a role in the earlier work.[21,24] We checked this possibility by deliberately raising the pressure in the excitation region. With the nozzle−laser beam distance x decreased from 27 to 7 mm, the measurement of slow and prompt fluorescence excitation spectra was repeated under otherwise identical conditions; see Figure 3c and 3d. The about 15 times increase in pressure has no effect on the prompt LIF spectrum, as a comparison of Figure 3d with 3b shows. The effect on the slow fluorescence spectrum, however, is dra-

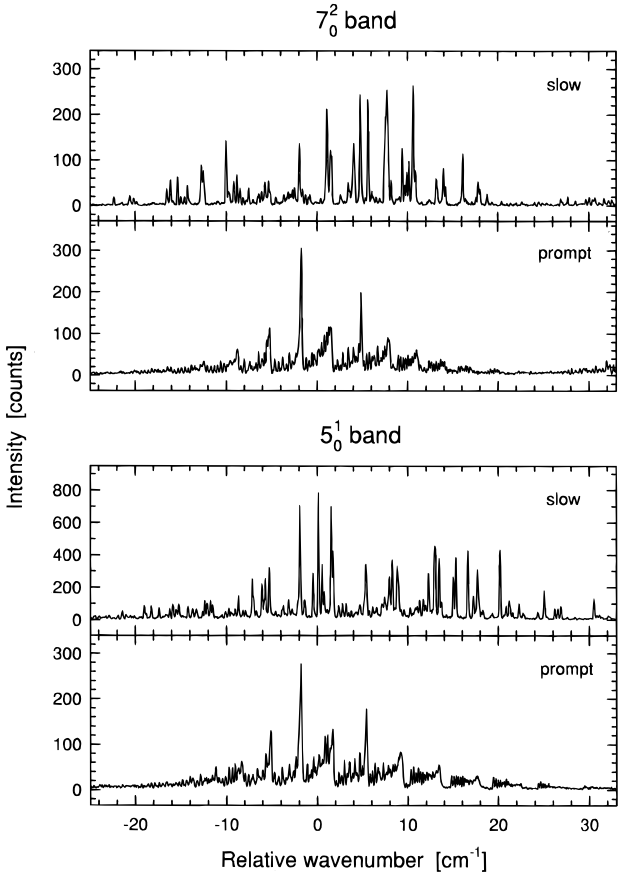

Figure 4. Slow and prompt fluorescence excitation spectra of the 7_0^2 (top) and 5_0^1 (bottom) bands. The excess energies are 463 cm^{-1} for 7_0^2 and 509 cm^{-1} for 5_0^1. Experimental conditions as in Figure 3, a and b. The intensity ratio of the highest peaks in the slow and prompt spectra can be estimated from the count rates and the attenuation factors as prompt/slow $\approx$ 1600 for 7_0^2 (top) and 1700 for 5_0^1 (bottom).

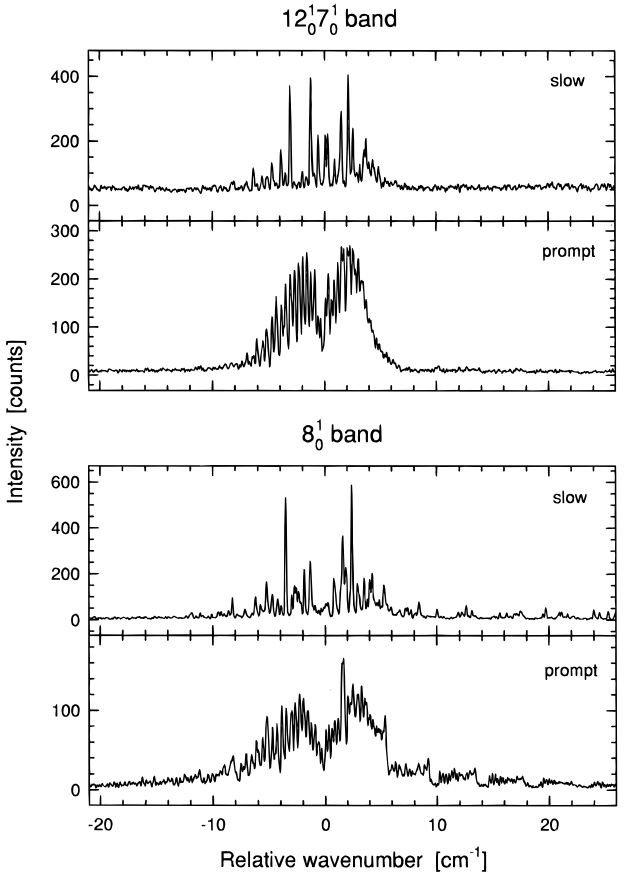

Figure 5. Same as Figure 4, for the $12_0^1 7_0^1$ and the 8_0^1 bands. The respective excess energies are 615 and 735 cm^{-1}. The intensity ratio of the highest peaks in the slow and prompt spectra can be estimated from the count rates and the attenuation factors as prompt/slow $\approx$ 250 for $12_0^1 7_0^1$ (top) and 650 for 8_0^1 (bottom).

matic: Figure 3c shows that the slow spectrum is now much more similar to the prompt spectra, Figure 3b or 3d, than to the collision-free slow spectrum, Figure 3a. It exhibits now the characteristic red degradation and pattern of band heads in the central part, as well as the compact, dense "blocks" of lines in the right-hand part of the spectrum. There are only some traces left of the unadulterated slow fluorescence spectrum, Figure 3a, e.g., the superimposed group of the three strong lines in the center, and another three lines near the right-hand end of the spectrum.

We consider this to be experimental proof that in both of the earlier studies, refs 21 and 24, collisional effects must have been responsible for the dense appearance of the phosphorescence spectra. Following the laser pulse, the excitation energy was largely randomized within the S_1 state by collisions. This will give almost any laser-excited level an equal chance of communicating with one of the few S_1/T_1 gateway levels and, thereby, acquiring a long lifetime. The phosphorescence excitation will then track closely with the primary S_1 excitation probability, as reflected by the fluorescence. Under these circumstances, it is not possible to identify the gateway levels from the excitation spectrum. It is informative to compare the nozzle expansion parameters of the three experiments. Jouvet and Soep[21] used a very small (35-μm-diameter) nozzle, but upwards from 10 bar of stagnation pressure, and the excitation region was only a few millimeters from the nozzle exit. Kamei et al.[24] worked at lower pressures (4 atm) and a larger distance from the nozzle (15 mm) but used a 800-μm-diameter nozzle. They do admit that the possibility of soft collisions cannot be denied. In fact, the figure of merit $Y = x^2/(pd^2)$ (x = distance of laser beam from the nozzle, p = stagnation pressure, d = nozzle diameter) is somewhat smaller in their experiment (Y = 67 bar^{-1}) than in Jouvet and Soep's ($Y \sim 200$ bar^{-1}). In the present experiment, the critical parameter was $Y \sim 6700$ bar^{-1}, for the distance $x = 27$ mm typically used. Only in the test experiment with $x = 7$ mm (Figure 3c and 3d) was $Y \sim 450$ bar^{-1}. This is still greater than in either ref 21 or 24; therefore, it is certain that in the two earlier investigations, the collisional effects were completely dominant.

Figures 4, 5, and 6 show high-resolution scans of six other bands, grouped together in pairs, in order of ascending excess energy. In each case, the slow and prompt fluorescence excitation spectra are shown for a nozzle/laser beam distance of 27 mm, i.e., corresponding to Figure 3a and 3b (collision-free conditions). Figure 4 shows the two-quantum excitation of the ν_7 acetyl group torsional mode (a_u symmetry) and of the ν_5 C—C═O bending mode (totally symmetric, a_g). Both are typical c-type perpendicular bands. The density of the slow fluorescence lines is considerably greater than in Figure 3a. This is as expected, since the density of accidental resonances between S_1 and T_1 levels should increase rapidly with the excess energy. The slow fluorescence of the 5_0^1 and 7_0^2 bands was examined for its pressure dependence similarly as is shown in Figure 3c for the 0_0^0 band. Again it was found that the density of lines increased markedly upon decreasing the distance x from 27 to 7 mm, and the overall contour of the slow bands became much more similar to that of the respective prompt bands. This shows that, as in the case of the 0_0^0 band and no doubt quite

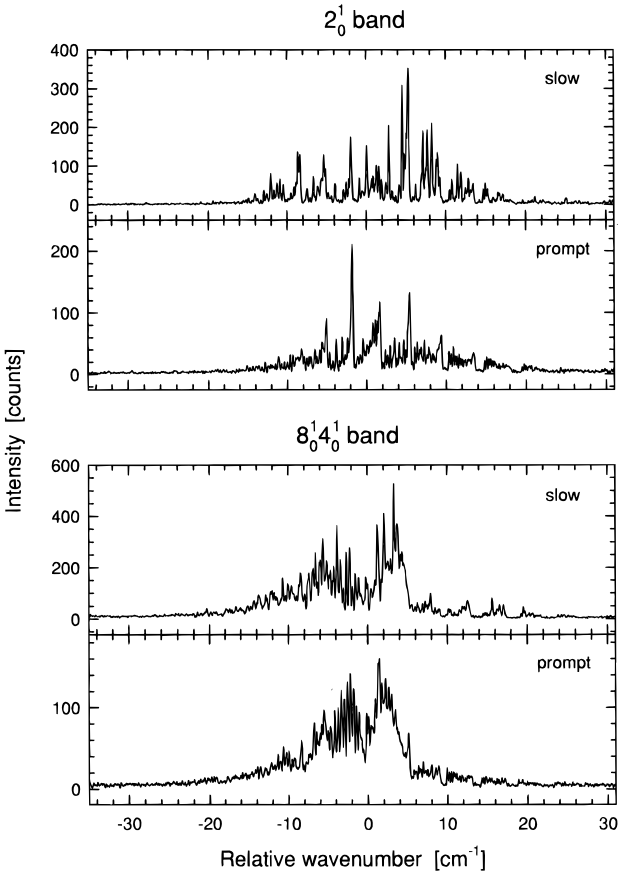

Figure 6. Same as Figure 4, for the 2_0^1 and $8_0^1\,4_0^1$ bands. The respective excess energies are 1391 and 1677 cm^{-1}. The intensity ratio of the highest peaks in the slow and prompt spectra can be estimated from the count rates and the attenuation factors as prompt/slow ≈ 580 for 2_0^1 (top) and ≈300 for $8_0^1\,4_0^1$ (bottom).

generally, extreme care has to be exercised if collisional effects on the long-lived emission are to be avoided.

Figure 5, top, shows the combination band of the $\nu_7(a_u)$ mode with the $\nu_{12}(b_u)$ C—C═O bending mode, having overall b_g symmetry. The band contour is that of an a-type parallel band. The 8_0^1 band shown in Figure 5, bottom, lies at a still somewhat higher energy (cf. Figure 2). It corresponds to excitation of the b_g C—H wagging mode, and the contour is of the a + b type, showing the characteristics of both parallel bands (the central minimum) and of perpendicular bands (e.g., the blocks of lines on the blue side). The density of slow fluorescence lines is moderately high in both spectra.

Figure 6 shows the ν_2 C═O stretch excitation (symmetry a_g) and the combination band of ν_8 with the totally symmetric C—C stretch vibration, ν_4. The former is c type, the latter a + b type. Both lie at rather high excess energies, and correspondingly, the density of slow fluorescence lines here is very large.

4. Discussion

4.1. Spectrum Simulation. For a quantitative analysis and identification of the slow fluorescence lines, some of the spectra were computer simulated. As a first step, simulations of the ordinary prompt fluorescence excitation spectra were done, using the program ASYSPEC. It calculates rotational line positions and line strengths for singlet—singlet vibronic transitions in asymmetric top molecules, excluding nuclear spin statistics. The experimental line width was taken into account. The rotational constants *A*, *B*, *C*, D_J, and D_K of the glyoxal S_0 and S_1 states, as well as the vibronic origins, were taken from ref 10. The

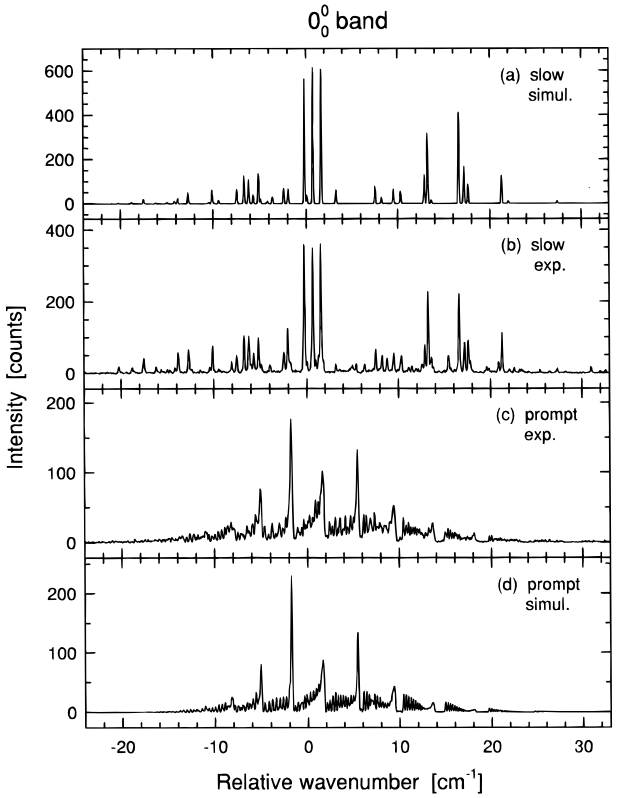

Figure 7. Simulated slow and prompt fluorescence excitation spectra (a and d) compared with the corresponding experimental results (b and c, reproduced from Figure 3a and 3b, respectively). For details of the simulation, see the text.

result for the 0_0^0 band is shown in Figure 7d. For greater ease of comparison, the corresponding experimental spectrum, Figure 3b, is reproduced in Figure 7c. It is seen that the calculated band contour matches the observed spectrum very well. The only adjustable parameters in the simulation were the line width and the rotational temperature. The experimental line width was adjusted, from a best visual fit, to be 0.12 cm^{-1}, or 3.6 GHz. The Doppler width alone is estimated to contribute ∼2 GHz. The laser bandwidth itself must then be ∼3 GHz, or 0.1 cm^{-1} (estimated from $\Delta\nu = (\Delta\nu_{\text{Doppler}}^2 + \Delta\nu_{\text{Laser}}^2)^{1/2}$). This is much better than the typical laser bandwidth specified by the manufacturer. The rotational temperature was chosen as T_{rot} = 15 K in the case of the 0_0^0 band, Figure 7, so as to give the best overall fit of the band contour.

It is noteworthy that it was possible to simulate the entire spectrum using a single rotational temperature. This is in stark contrast to the results reported in ref 11, where very different T_{rot} values were obtained for lines belonging to different *K* values. According to that work, T_{rot} varied from 1.2 to 20 K in going from $K = 0$ and 1 to $K = 12-15$. It is likely that in this experiment, the rotational relaxation during the expansion was incomplete, since the laser excitation region was located very close (1 mm) to the 50-μm nozzle. Although the authors claim that this was "outside the collision region" (despite the high stagnation pressure of 10 bar of He used), their results suggest strongly that only molecules in low-*K* levels were approximately fully relaxed. The high-*K* states, on the other hand, apparently did not reach the equilibrium T_{rot}. Considering the prolate symmetry of the glyoxal molecule, it is quite plausible that the cross section for rotationally inelastic collisions is significantly smaller if the axis of rotation is close to the figure axis, i.e., for high-*K* states.

Having verified that the computer program can indeed reproduce the experimental results, we proceeded to simulate

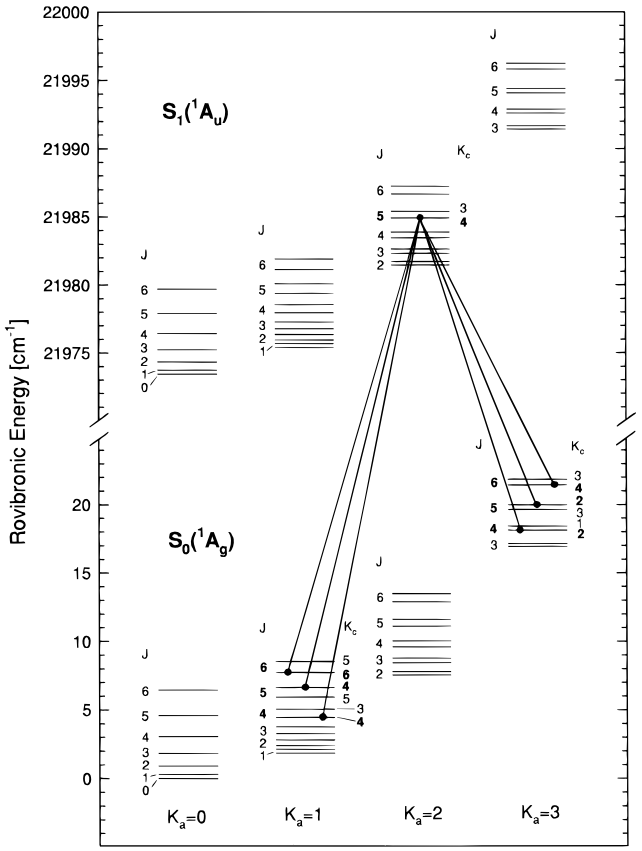

Figure 8. Schematic rotational level diagram of the slightly asymmetric rotor glyoxal S_0 and S_1. K_a is the projection of the total angular momentum J onto the "long" (O−C−C−O) axis of the molecule. Due to the slight deviation from a prolate symmetric top, all levels with $K_a > 1$ are split, the index K_c indicating the projection of J on the c axis in the limiting case of an oblate top. Alternative designations are K_{-1} for K_a and K_1 for K_c. The selection rules for the perpendicular electronic transition $n\pi^*$ $^1S_1(^1A_u) \leftarrow {}^1S_0(^1A_g)$ are $\Delta J = 0, \pm 1$, $\Delta K_a = \pm 1$, $\Delta K_c = 0, \pm 2$, allowing up to six transitions into a given upper state level.

the slow fluorescence spectra. The only, but decisive, difference was that the emitting levels were now no longer populated according to a Boltzmann distribution. In the case of the slow fluorescence spectra, only a few excited state rotational levels contribute, namely, those that possess an anomalously long lifetime through accidental wave function mixing with the T_1 state. For any given S_1 level, the probability will be small that a T_1 level lies nearby (within the width of the S/O matrix element) and fulfills the selection rules for intramolecular S/O coupling. Thus, only a small fraction of all laser-excited S_1 levels will actually have an appreciable admixture of T_1 character in their wave function. Correspondingly, the slow fluorescence spectra will consist of a small fraction of the lines making up the full, prompt fluorescence spectra. This sample will have a quasi-random distribution of the rotational quantum numbers as well as of the intensities.

Comparing the observed slow fluorescence rotational line positions with the simulated spectra, it is possible to identify precisely those particular S_1 rovibronic levels from which the long-lived fluorescence originates. Due to the high density of rotational lines in the simulated spectra, there are, however, typically 5−10 calculated lines which fall within the experimental 0.12-cm^{-1} width of each observed slow fluorescence line. In order to select the correct assignment out of these various possibilities, one takes advantage of the fact that up to six transitions exist which lead from the ground state into a given upper level. This is illustrated in Figure 8. For each of the 5−10 trial assignments, the entire multiplet pattern of such lines sharing the same assumed upper state level was calculated. Then the requirement for the correct assignment was that *all* these lines be actually observed with an appropriate intensity ratio. In this way, it was straightforward, although tedious, to eliminate all false assignments among the candidates initially considered. This procedure led to the results compiled in Table 1 for the 0_0^0 band. Ten long-lived rovibronic levels could be uniquely identified with regard to J' and K_a'. Moreover, the quantum number K_c', typical of an asymmetric top, could be determined for all levels with $K_a' \leq 2$. An ambiguity of K_c' remains only for levels having $K_a' \geq 4$. Here the levels belonging to the two possible K_c' values are very nearly degenerate, both in the S_0 and S_1 states, especially since glyoxal is an only slightly asymmetric rotor. In these cases, the entire group of lines calculated for the same upper state level agreed with the observed line pattern for both possible K_c' values, within the experimental line widths. The K_c' alternatives could therefore not be distinguished. The J' and K_a' levels are distributed over the ranges $J' = 1-20$ and $K_a' = 0-7$, with no apparent regularity. It is useful to relate this to the thermal distribution of the J and K_a levels in the ground state. This can be assessed from the $I(T)_{calc}$ values given in Table 1. We compare, for example, the Q(J), $\Delta K = +1$ lines for $K_a' = 1$ (i.e., $K_a'' = 0$). From Table 1, the $I(T)_{calc}$ values for $J = 4$, 12, 17, and 20 are 53.3, 22.4, 3.9, and 0.4. This indicates the experimentally accessible range and shows that the observed gateway levels cover it rather uniformly. Similarly, from Table 2, the corresponding $I(T)_{calc}$ distribution for $J = 1$, 5, and 15 is 4.2, 12.8, and 9.1.

With this information, it was then possible also to simulate the slow fluorescence spectra. Contrary to the prompt fluorescence simulation, the emission intensity distribution in this case was not simply determined by the relative population of the emitting levels, as derived from the ground-state thermal distribution and the relative absorption probabilities. Although these latter factors do enter in the same way as for the prompt fluorescence, the decisive additional parameter is the fractional triplet character of the emitting levels, which controls the lifetime lengthening. This triplet admixture is a quantity which at present cannot be calculated ab initio. The analysis described above yields only a complete characterization of the emitting singlet levels, in terms of quantum numbers and term energy. The dark triplet levels to which they are coupled are, however, not known, nor is the strength of the coupling. The coupling strength depends not only on the S/O matrix element but particularly sensitively on the precise relative position of the interacting energy levels. In the region of fairly high vibrational excitation within the T_1 manifold considered here, the triplet level density will be very high. In addition, the spectroscopic information on T_1 glyoxal is limited. For these reasons, the exact T_1 levels responsible for the slow fluorescence observed here have to remain unidentified.

The slow fluorescence emission intensity from each mixed S_1/T_1 level was represented in the simulation by a separate fit parameter $\bar{\gamma}$. It relates the observed, "slow" intensities I_{exp} to the theoretical intensities I_{calc}, as calculated without regard for the randomly varying S_1/T_1 coupling strength. Thus, in the case of the 0_0^0 band, 10 such numbers $\bar{\gamma}$ had to be determined. $\bar{\gamma}$ is obtained as the average of the individual ratios $\gamma = I_{exp}/I_{calc}$ for each line of the multiplet; see Table 1. Here I_{exp} is given as the integrated line intensity, in units of counts times wavenumber. (A typical line width of $\gtrsim$0.12 cm^{-1} covers about 5 data points in the high-resolution scan mode; see section 2.) The calculated intensity, I_{calc}, listed in Table 1 is the result given by the computer program for the rotational temperature derived

TABLE 1: Long-Lived Levels in the Vibrationless Glyoxal S_1 State and the Corresponding Observed Lines in the $S_1 \leftarrow S_0$ Excitation Spectrum

emitting level[a]	ΔJ	ΔK_a	ΔK_c[b]	$\tilde{\nu}_{exp}$,[c] cm^{-1}	$\tilde{\nu}_{calc}$, cm^{-1}	I_{exp},[d] cts cm^{-1}	$I(T)_{calc}$,[e] rel units	γ [f]	$\bar{\gamma}$ [g]
$J' = 11, K_a' = 4, K_c' = 7$ (8)	R(10)	+1	0 (0)	21 990.03	21 990.07	38.9	3.5	11.1	
	Q(11)	+1	−2 (0)	21 986.67	21 986.68	42.3	2.7	15.7	
	P(12)	+1	−2 (−2)	21 982.97	21 982.99	8.6	0.54	15.9	*15*
	R(10)	−1	+2 (+2)	21 963.02	21 963.02	1.1	0.05	(22)	
	Q(11)	−1	0 (+2)	21 959.61	21 959.64	10.6	0.19	55.8*	
	P(12)	−1	0 (0)	21 955.92	21 955.95	7.3	0.16	45.6*	
$J' = 14, K_a' = 4, K_c' = 10$ (11)	R(13)	+1	0 (0)	21 990.61	21 990.64	15.1	1.4	(10.8)	
	Q(14)	+1	−2 (0)	21 986.32	21 986.33	13.8	1.1	12.5	
	P(15)	+1	−2 (−2)	21 981.71	21 981.71	6.8	0.23	(29.6)	*15*
	R(13)	−1	+2 (+2)	21 963.51	21 963.60	0.68	0.03	(22.7)	
	Q(14)	−1	0 (+2)	21 959.28	21 959.30	1.6	0.08	20	
	P(15)	−1	0 (0)	21 954.65	21 954.68	1.8	0.05	(36)	
$J' = 17, K_a' = 1, K_c' = 17$	Q(17)	+1	0	21 973.19	21 973.27	68.1	3.9	17.5	
	R(16)	−1	+2	21 971.40	21 971.50	26.7	0.46	(58.0)	*18*
	Q(17)	−1	+2	21 965.95	21 966.03	7.9	0.45	17.6	
	P(18)	−1	0	21 960.73	21 960.76	10.4	0.26	(40.0)	
$J' = 12, K_a' = 5, K_c' = 7$ (8)	R(11)	+1	0 (0)	21 994.72	21 994.77	16.0	0.95	16.8	
	Q(12)	+1	−2 (0)	21 991.02	21 991.08	20.5	0.64	(32.0)	
	P(13)	+1	−2 (−2)	21 987.05	21 987.08	4.2	0.11	(38.2)	*17*
	R(11)	−1	+2 (+2)	21 961.08	21 960.97	0.35	0.006	(58.2)	
	Q(12)	−1	0 (+2)	21 957.25	21 957.28	2.5	0.02	(106.5)	
	P(13)	−1	0 (0)	21 953.22	21 953.28	2.9	0.02	(136.2)	
$J' = 12, K_a' = 1, K_c' = 12$	Q(12)	+1	0	21 974.10	21 974.18	70.0	22.4	3.1	
	R(11)	−1	+2	21 970.98	21 971.05	9.3	2.5	3.7	*3.5*
	Q(12)	−1	+2	21 967.23	21 967.29	14.1	3.9	3.6	
	P(13)	−1	0	21 963.35	21 963.37	10.9	2.2	(5.0)	
$J' = 4, K_a' = 1, K_c' = 4$	Q(4)	+1	0	21 975.00	21 975.11	74.7	53.3	1.4	
	R(3)	−1	+2	21 969.48	21 969.58	3.8	2.5	1.5	*1.45*
	Q(4)	−1	+2	21 968.26	21 968.34	15.1	11.9	1.3	
	P(5)	−1	0	21 966.74	21 966.81	17.4	11.0	1.6	
$J' = 20, K_a' = 1, K_c' = 19$	R(19)	+1	0	21 980.99	21 981.02	9.8	0.4	24.5	
	P(21)	+1	−2	21 968.56	21 968.59	2.0	0.11	(18.2)	
	R(19)	−1	+2	21 973.47	21 973.54	2.2	0.19	(11.6)	*25*
	Q(20)	−1	0	21 967.77	21 967.79	5.9	0.2	(29.5)	
	P(21)	−1	0	21 960.73	21 960.79	10.4	0.08	(130)	
$J' = 12, K_a' = 7, K_c' = 5$ (6)	R(11)	+1	0 (0)	22 004.45	22 004.53	2.5	0.05	50	
	Q(12)	+1	−2 (0)	22 000.83	22 000.84	1.6	0.02	80	*65*
$J' = 16, K_a' = 5, K_c' = 11$ (12)	R(15)	+1	0 (0)	21 995.51	21 995.49	1.2	0.2	6	
	Q(16)	+1	−2 (0)	21 990.61	21 990.56	15.1	0.2	(75.5)	*6*
$J' = 17, K_a' = 2, K_c' = 16$	R(16)	+1	0	21 983.78	21 983.76	10.5	1.2	8.8	
	Q(17)	+1	0	21 976.64	21 976.74	3.1	1.3	2.4	
	P(18)	+1	−2	21 973.19	21 973.24	?	0.30	(?)	*6*
	R(16)	−1	+2	21 969.26	21 969.31	0.4	0.21	1.9	
	Q(17)	−1	+2	21 964.01	21 964.07	1.3	0.31	4.2	
	P(18)	−1	0	21 958.45	21 958.54	1.2	0.14	8.6	

[a] K_c' values in parentheses are alternatives which are experimentally indistinguishable. [b] The values in parentheses refer to the K_c' values given in parentheses in column 1. [c] Vacuum wavenumber. [d] Area under the line profile. [e] Line intensity calculated for a temperature T (see the text).[f] $\gamma = I_{exp}/I(T)_{calc}$. Values in parentheses are uncertain because of line blends. Values marked with an asterisk are numerically uncertain because of a very small value of $I(T)_{calc}$. [g] γ for each emitting level, averaged over the values listed in the preceding column with the exception of those in parentheses or marked with an asterisk.

from the prompt fluorescence spectrum (15 K in the case of the 0_0^0 band).

In order to be able to transfer the T_{rot} value measured in the prompt fluorescence spectrum to the corresponding slow fluorescence spectrum, one has to be certain that T_{rot} is reproducible for different experiments on the same band. Changing between fast and slow detection involves repositioning the photomultiplier and, hence, breaking the vacuum. After turning the gas flow off and on again, it is difficult to reset the glyoxal and seed gas pressures precisely. However, identical T_{rot} values were obtained in repeated test runs on the prompt fluorescence of a given band, despite the possibly slightly different expansion conditions.

The ratio $I_{exp}/I_{calc} = \gamma$ given in Table 1 is subject to large experimental uncertainties. Within each multiplet of up to six lines, γ should be the same for each line. This is not what is found. In some cases, marked by an asterisk, the line appears to be blended, judging by its broadened or asymmetric profile. In other cases, γ is exceptionally large for no such obvious reason. Maybe here, too, unidentified underlying line components are present. In determining the average $\bar{\gamma}$ for each multiplet, only the strong observed lines were utilized. Weak or blended lines, as well as lines with large I_{exp} but small I_{calc} (i.e., with an abnormally large γ value), were excluded from the averaging. A comparison of the $\bar{\gamma}$ values obtained for each multiplet indicates qualitatively which emitting levels are particularly strongly coupled to the T_1 manifold. A large value of $\bar{\gamma}$ corresponds to a relatively large admixture of T_1 character into the S_1 wave function.

The simulated slow fluorescence spectrum of the 0_0^0 band was finally obtained by superimposing, with the relative weights $\bar{\gamma}$, the calculated line patterns of the 10 contributing multiplets. The result is shown in Figure 7a. For a convenient comparison, in Figure 7b, the experimentally determined slow fluorescence spectrum from Figure 3a has been reproduced. It can be seen that the result is very satisfactory. It fully confirms our assignment of the 10 rotational levels of glyoxal in the vibrationless S_1 state which have an anomalously long lifetime.

TABLE 2: Long-Lived Levels in the ν_5 Vibronic Level of the Glyoxal S_1 State and the Corresponding Observed Lines in the $S_1 \leftarrow S_0$ Excitation Spectrum[a]

emitting level[a]	ΔJ	ΔK_a	ΔK_c[b]	$\tilde{\nu}_{exp}$,[c] cm^{-1}	$\tilde{\nu}_{calc}$, cm^{-1}	I_{exp},[d] cts cm^{-1}	$I(T)_{calc}$,[e] rel units	γ [f]	$\bar{\gamma}$ [g]
$J' = 5, K_a' = 1, K_c' = 5$	Q(5)	+1	0	22 483.94	22 483.98	98.8	12.8	7.7	
	R(4)	−1	+2	22 478.69	22 478.75	13.7	1.0	(13.7)	*10*
	Q(5)	−1	+2	22 477.14	22 477.21	47.7	4.0	11.9	
	P(6)	−1	0	22 475.28	22 475.37	16.5	3.5	(4.7)	
$J' = 1, K_a' = 1, K_c' = 1$	Q(1)	+1	0	22 484.14	22 484.18	61.5	4.2	(14.6)	
	P(2)	−1	0	22 476.72	22 476.80	38.8	2.9	13.4	*13*
$J' = 10, K_a' = 0, K_c' = 10$	R(9)	−1	+2	22 482.93	22 482.98	64.3	5.4	11.9	
	Q(10)	−1	0	22 480.50	22 480.54	138.1	13.4	(10.3)	*9*
	P(11)	−1	0	22 476.33	22 476.40	33.5	5.4	6.2	
$J' = 11, K_a' = 2, K_c' = 9$	R(10)	+1	0	22 490.38	22 490.41	46.1	4.6	(10.0)	
	Q(11)	+1	−2	22 487.77	22 487.79	82.7	4.8	(17.2)	
	P(12)	+1	−2	22 483.16	22 483.21	∼30	2.1	(∼15)	*8*
	R(10)	−1	+2	22 477.14	22 477.22	?	1.0	(?)	
	Q(11)	−1	0	22 473.75	22 473.84	19.3	2.8	6.9	
	P(12)	−1	0	22 470.03	22 470.14	17.4	1.9	9.2	
$J' = 15, K_a' = 1, K_c' = 15$	Q(15)	+1	0	22 482.53	22 482.59	116.7	9.1	12.8	
	R(14)	−1	+2	22 480.25	22 480.29	∼20	1.2	(∼17)	*13*
	Q(15)	−1	+2	22 475.45	22 475.53	∼10	1.8	(∼6)	
	P(16)	−1	0	22 470.65	22 470.78	16.7	1.2	13.9	
$J' = 6, K_a' = 4, K_c' = 2$ (3)	R(5)	+1	0 (0)	22 497.71	22 497.71	61.3	4.1	15.0	
	Q(6)	+1	−2 (0)	22 495.86	22 495.86	63.2	2.3	27.5	
	P(7)	+1	−2 (−2)	22 493.71	22 493.71	13.5	0.4	33.8	*22*
	Q(6)	−1	0 (+2)	22 468.68	22 468.82	11.7	0.5	23.4	
	P(7)	−1	0 (0)	22 466.52	22 466.66	14.5	1.2	12.1	

[a] For the footnotes, see Table 1.

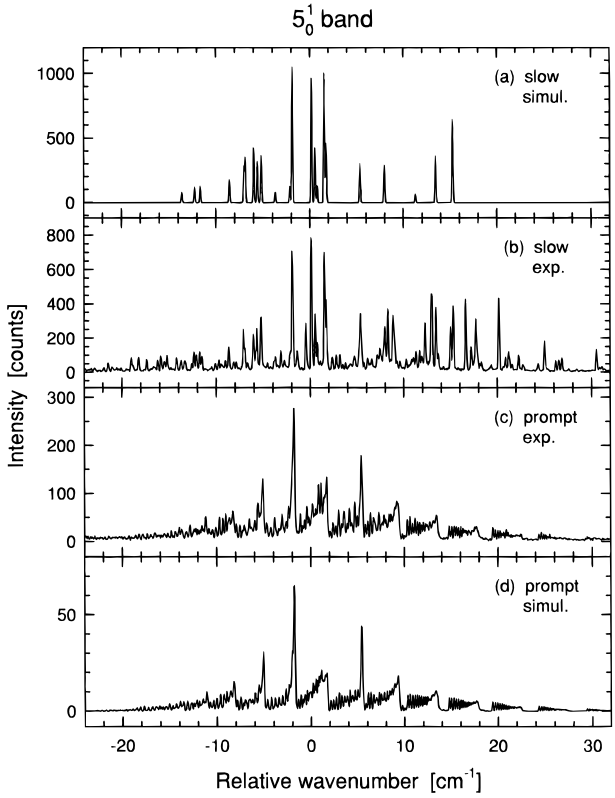

Figure 9. Same as Figure 7, for the 5_0^1 band. The experimental spectra, b and c, here are reproduced from Figure 3, bottom half. The "slow" simulation is incomplete.

It is also seen that this set of 10 levels encompasses the great majority of the perturbed S_1, $v = 0$ levels, since they can account for practically all significant features of the observed slow fluorescence spectrum.

A similar analysis was performed for the prompt and slow fluorescence spectra of the 5_0^1 vibrational band, Figure 4, bottom half. The results are shown in Figure 9, in the same format as Figure 7. The prompt spectrum was simulated using a rotational temperature of 30 K, twice the value for the 0_0^0 band. This difference is certainly outside the error limits of the simulation. It is also not an experimental artifact, since for repeated measurements of the same band, T_{rot} was always reproducible (see above). One explanation might be that the rotational line strengths (Hönl−London factors) are somewhat different for bands of different vibronic symmetry.

The slow fluorescence excitation spectrum of the 5_0^1 band is shown in Figure 9b. It exhibits a much greater number of lines than the corresponding spectrum of the 0_0^0 band, Figure 7b. This is due to the excess energy over the S_1 origin in the former case. At the higher energy, the level density in the T_1 manifold is much greater, and far more possibilities for S/O coupling between S_1 and T_1 levels exist. Figure 9a shows a partial simulation of the experimental spectrum, Figure 9b. In view of the complexity of the latter, a complete simulation, such as was almost achieved in the case of the 0_0^0 band (Figure 7a), was not attempted here. With the much greater line density in the present case, ambiguous assignments are more frequent. None of these were admitted among the final results. Nevertheless, most of the principal features have been identified correctly. The analysis includes in this case 6 upper state levels and 24 lines, as listed in Table 2.

Simulations of the prompt and the slow fluorescence were also done for the 7_0^2 band but are not shown here. The former was of similar quality as for the 0_0^0 and 5_0^1 bands (Figures 7d and 9d), and yielded $T_{rot} = 25$ K. The experimental slow fluorescence spectrum is quite dense, similar to that of the 5_0^1 band, Figure 9b (compare Figure 4, top and bottom half). In this case, however, even a partial simulation met with difficulties. It was not possible to identify multiplets of lines which clearly belonged to the same upper state level. There is no obvious reason for this.

4.2. Relative Fluorescence Intensities. It may be useful to give some indication of the relative intensities of the 0_0^0 bands of (a) the $T_1 \leftarrow S_0$ LIP excitation spectrum (Figure 1), (b) the slow LIF excitation spectrum (Figures 1 and 3a), and (c) the prompt LIF excitation spectrum (Figure 3b). Regarding a and b, Figure 1 does not give the correct relative intensities because of the signal saturation. However, in another experi-

ment carefully checked for saturation effects,[29] the LIP excitation spectrum of the $T_1 \leftarrow S_0$ 0_0^0 band was observed at high resolution. Comparing the count rate of the highest peak in the spectrum with that for the corresponding high-resolution, saturation-free slow LIF spectrum in Figure 3a, each normalized to the respective laser pulse energies, one finds an intensity ratio b/a $\sim$ 25. The intensity ratio c/b can be derived from the data shown in Figure 3. Taking into account the attenuation by filters placed in the laser beam (5×10^{-5} for Figure 3a, 5×10^{-8} for Figure 3b), an intensity ratio c/b $\sim$ 470 is obtained for the respective highest peaks. This value is typical; for all 17 investigated $S_1 \leftarrow S_0$ bands with 2 exceptions, the intensity factor between the prompt and slow emission was on the order of 250−650, without any regularity.

The exceptions are the 7_0^2 and 5_0^1 bands, where the corresponding ratios of the prompt and slow fluorescence intensities were 1600 and 1700, respectively. The deviation from the average for the other 15 bands is, however, not significant, in view of the fact that all stated intensity ratios refer, somewhat arbitrarily, only to the highest peaks in the spectra; the very different line densities and structure of the slow and prompt fluorescence spectra are disregarded. An alternative representation would have been a comparison of the integrated band intensities. This, however, has the disadvantage that it complicates the comparison of bands whose prompt fluorescence spectra have a different structure, e.g., c type as shown in Figure 4 vs a or a + b type as in Figure 5.

Regarding the 7_0^2 and 5_0^1 bands, this objection does not apply, since here the structures of the two prompt fluorescence spectra as well as the line densities in the two slow fluorescence spectra are very similar; see Figure 4. Consequently, a comparison of integral band intensities is meaningful here. It is found that the ratio $I_{\text{prompt}}/I_{\text{slow}}$ (integral), including the experimental excitation conditions as before, is 2000 for the 7_0^2 band and 2100 for the 5_0^1 band. Thus, the relative intensities are, in fact, very similar, justifying in retrospect the above comparison of the peak intensities.

More important, however, is the fact that this result is in contradiction to observations which were made by the Ito group.[23] Here the ratio of the sensitized phosphorescence intensity to the (prompt, <13-μs delay) fluorescence intensity was investigated systematically for a large number of vibrational modes of glyoxal (as well as methylglyoxal and biacetyl). Ito's data are essentially ratios of integral band intensities, since the spectra were not rotationally resolved in that work. It was found that quite generally, modes involving the ν_7 out-of-plane vibration had a much higher phosphorescence yield, relative to the fluorescence yield, than did the totally symmetric vibrations. The conclusion was that the torsional mode greatly promotes the $S_1 \rightarrow T_1$ intersystem crossing. Among the three molecules studied, the effect was most pronounced in glyoxal. For the 7_0^2 band of glyoxal, the phosphorescence/fluorescence ratio is stated to be about 10 times greater than for the 5_0^1 band (ref 23, Figure 3). This is at variance with our results given above. We find quite similar relative intensities for these two bands, although the 7_0^2 band involves an out-of-plane mode, while the 5_0^1 band does not. Thus, we cannot confirm the mode selectivity in intersystem crossing claimed by the Ito group.[23] Likewise, the $12_0^1 7_0^1$ and $6_0^1 7_0^1$ combination bands (Figure 2), which also involve the ν_7 out-of-plane mode, did not show an anomalously enhanced slow fluorescence yield in our experiment.

For an explanation of the discrepancy with Ito's results, one has to bear in mind that in Ito's work, the ISC process was most likely mediated through collisions, while we observed for the first time the truly collision-free, unimolecular $S_1 \rightarrow T_1$ radiationless transitions. In ref 23, the possible contribution of collisions is not explicitly commented on, but the experimental conditions were similar to those used in ref 24, where we have shown above that collisional effects were dominant, at least as far as the rotational structure is concerned. The nozzle−laser beam distance used in ref 23 was, in fact, smaller than in ref 24 (10 vs 15 mm, with otherwise identical expansion conditions) so that collisional effects must have been even stronger in this case. Our results show that neither is the S_1/T_1 coupling strength increased by the participation of the out-of-plane mode nor is the number of contributing gateways. The latter fact is evidenced by the comparable line densities of the slow fluorescence spectra in Figure 4, 7_0^2 and 5_0^1.

The large factor of (at least) about 500 between the yields of slow and prompt fluorescence can be due to two reasons: (i) An excited perturbed level may be predominantly S_1 in character, with only a small T_1 admixture. The $S_1 \leftarrow S_0$ excitation probability will then be almost as high as for an unperturbed S_1 level, and the lifetime will be only slightly greater than the pure S_1 lifetime of 2.4 μs. One can easily calculate that with a lifetime of $\sim$4.5 μs, 2×10^{-3} of the total emission will occur within the experimental time window, from 30 to 80 μs after the laser pulse. (ii) The excited level may be predominantly T_1 in character, with a correspondingly low excitation probability, but a very long radiative lifetime. Again, the S_1/T_1 mixing may be such that the intensity emitted within the observation window is about 2×10^{-3} of the normal, prompt fluorescence from the unperturbed, pure S_1 levels. Since any perturbation produces a pair of "mirror image" states, one predominantly S_1 and the other predominantly T_1, the two situations may be about equal in number. Experimentally, they can be distinguished by moving the detection gate toward longer delays: In case i, this will reduce the slow fluorescence intensity drastically, while in case ii, it will not change much. We have preliminary evidence of this. A few slow fluorescence excitation spectra of the 0_0^0, 5_0^1, and 7_0^2 bands were taken with greater delay and a larger distance from the excitation to the observation region. These spectra were again very sparse and showed essentially the same lines as in the two slow panels of Figure 4 but with very different relative intensities. This, if verified, would substantiate further the expected erratic variation of radiative lifetimes from one rotational line to another in the same band. Further experiments to this end are planned.

4.3. Hot Bands. Among the stronger prompt fluorescence bands shown in Figure 2, there is one hot band, labeled 7_1^1. It is remarkably intense, although this may be expected for a transition out of a low-lying vibrational level in the S_0 state (ν_7 = 127 cm^{-1}). However, this band is also abnormally broad, compared with, for example, the similarly strong 7_0^4 band. We therefore studied the 7_1^1 band at high resolution, both in the slow and in the prompt fluorescence mode. The results are shown in parts a and b of Figure 10, respectively. The simulation of the prompt fluorescence, shown in Figure 10c, required the unusually high rotational temperature of 70 K. It is interesting that among all the bands recorded at high resolution, it is only this vibrationally "hot" band which is also rotationally hot. This indicates that the incomplete collisional relaxation extends not only to the vibrational mode, in this case the torsional vibration, but to the quantum numbers K and J of the overall molecular rotation as well. The slow fluorescence excitation spectrum is, in this case, very complex. This is probably a direct consequence of the high rotational excitation, which makes a great number of gateway states accessible. No simulation of this slow fluorescence spectrum was attempted.

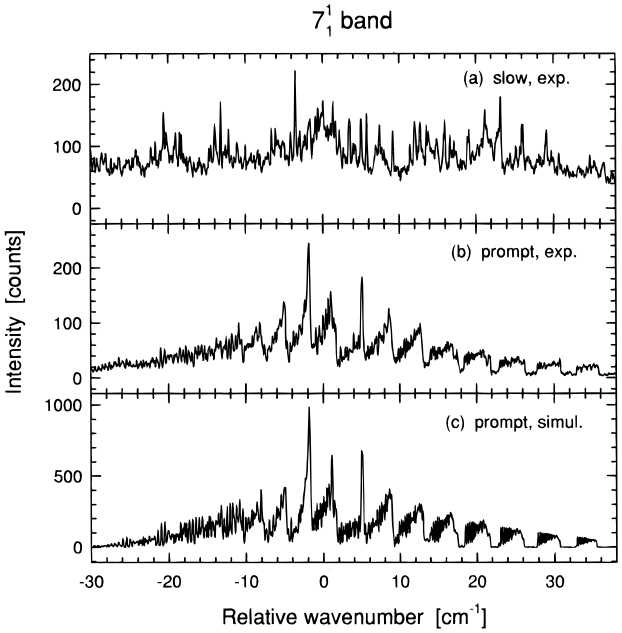

Figure 10. (a and b) Slow and prompt fluorescence excitation spectra of the 7_1^1 hot band. (c) Simulated prompt fluorescence excitation spectrum, yielding the unusually high rotational temperature of $T_{rot} =$ 70 K. The intensity ratio of the highest peaks in spectra a and b can be estimated from the count rates and the attenuation factors as b/a $\approx$ 350.

5. Conclusions

In this work, we have demonstrated the existence of certain very specific rovibrational levels in the first excited singlet state of glyoxal which have anomalously long radiative lifetimes. This is caused by accidental near-degeneracy of these $S_1(^1A_u)$ levels with levels of suitable symmetry in the $T_1(^3A_u)$ manifold, allowing mutual S/O perturbation. The resulting mixing of wave functions lends some triplet character to the zero-order singlet levels in question, thereby lengthening their radiative lifetime. This effect was observed in the S_1 vibrational ground state as well as in various vibrationally excited levels of S_1. A considerable number of perturbed levels was identified uniquely in terms of quantum numbers J, K_a, and K_c. To this end, a computer simulation of the $S_1 \leftarrow S_0$ transition was performed. Among the many calculated lines, those few could then be picked out and assigned which are distinguished by their anomalously slow fluorescence.

The significance of perturbed levels such as have been observed here lies in the fact that they serve as gateways, coupling the singlet and triplet manifolds of intermediate case molecules. In the absence of collisions, this coupling manifests itself in a biexponential decay, and a reduced quantum yield, of S_1 fluorescence. Furthermore, the much discussed collisional quenching of S_1 fluorescence by spinless particles such as rare gas atoms is also thought to proceed via pairs of S/O coupled levels in the S_1 and T_1 states. Although such collisional intersystem crossing has usually been considered in the $S_1 \rightarrow T_1$ direction, the reverse ISC, from T_1 to S_1, is also possible and will likewise be mediated by the gateway level pairs. We have, in fact, already observed collision-induced $S_1 \leftarrow T_1$ transitions, which is the first such observation in the gas phase (ref 29; see also ref 33). In these experiments, the initial state, T_1, was well below the S_1 state, making the overall process strongly endothermic. The collisions raise the molecule from the laser-excited, well-characterized T_1 level within the T_1 manifold to the as yet unspecified T_1 gateway levels in the region of the S_1 state. S/O coupling and the corresponding state mixing then lead to the observed $S_1 \rightarrow S_0$ fluorescence.

The present experiment has helped to shed more light on this process by a detailed examination of the gateways on the side of the S_1 manifold. The partner levels in the T_1 manifold, however, still remain to be identified. As a first step in this direction, we have recently spectrally resolved the slow fluorescence reported here (ref 29; see also ref 33).

Acknowledgment. J.H. and A.V. thank the Alexander von Humboldt-Stiftung for financial support.

References and Notes

(1) Rice, S. A. *Adv. Chem. Phys.* **1981**, *47*, 237.
(2) Freed, K. F. *Adv. Chem. Phys.* **1981**, *47*, 291.
(3) Tramer, A.; Nitzan, A. *Adv. Chem. Phys.* **1981**, *47*, 337.
(4) Brand, J. C. D. *Trans. Faraday Soc.* **1954**, *50*, 431.
(5) Gelbart, W. M.; Freed, K. F. *Chem. Phys. Lett.* **1973**, *18*, 740.
(6) Freed, K. F. *Chem. Phys. Lett.* **1976**, *37*, 47.
(7) Lombardi, M.; Jost, R.; Michel, C.; Tramer, A. *Chem. Phys.* **1980**, *46*, 273.
(8) Konings, J. A.; Majewski, W. A.; Matsumoto, Y.; Pratt, D. W.; Meerts, W. L. *J. Chem. Phys.* **1988**, *89*, 1813.
(9) Paldus, J.; Ramsay, D. A. *Can. J. Phys.* **1967**, *45*, 1389.
(10) Birss, F. W.; Brown, J. M.; Cole, A. R. H.; Lofthus, A.; Krishnamachari, S. L. N. G.; Osborne, G. A.; Paldus, J.; Ramsay, D. A.; Watmann, L. *Can. J. Phys.* **1970**, *48*, 1230.
(11) Pebay Peyroula, E.; Jost, R. *J. Mol. Spectrosc.* **1987**, *121*, 167.
(12) Anderson, L. G.; Parmenter, C. S.; Poland, H. M.; Rau, J. D. *Chem. Phys. Lett.* **1971**, *8*, 232.
(13) Anderson, L. G.; Parmenter, C. S.; Poland, H. M. *Chem. Phys.* **1973**, *1*, 401.
(14) Beyer, R. A.; Zittel, P. F.; Lineberger, W. C. *J. Chem. Phys.* **1975**, *62*, 4016.
(15) Beyer, R. A.; Lineberger, W. C. *J. Chem. Phys.* **1975**, *62*, 4024.
(16) Michel, C.; Lombardi, M.; Jost, R. *Chem. Phys.* **1986**, *109*, 357.
(17) Lapierre, L.; Dai, H. *J. Chem. Phys.* **1992**, *97*, 711.
(18) Parmenter, C. S.; Poland, H. M. *J. Chem. Phys.* **1969**, *51*, 1551.
(19) Küttner, H. G.; Selzle, H. L.; Schlag, E. W. *Chem. Phys.* **1978**, *28*, 1.
(20) Michel, C.; Tramer, A. *Chem. Phys.* **1979**, *42*, 315.
(21) Jouvet, C.; Soep, B. *J. Chem. Phys.* **1980**, *73*, 4127.
(22) Abe, H.; Kamei, S.; Mikami, N.; Ito, M. *Chem. Phys. Lett.* **1984**, *109*, 217.
(23) Kamei, S.; Okuyama, K.; Abe, H.; Mikami, N.; Ito, M. *J. Phys. Chem.* **1986**, *90*, 93.
(24) Kamei, S.; Mikami, N.; Ito, M. *J. Phys. Chem.* **1986**, *90*, 2321.
(25) Spangler, L. H.; Matsumoto, Y.; Pratt, D. W. *J. Phys. Chem.* **1983**, *87*, 4781.
(26) Ottinger, Ch.; Vilesov, A. F.; Winkler, T. *Chem. Phys. Lett.* **1993**, *208*, 299.
(27) Ottinger, Ch.; Vilesov, A. F. *Chem. Phys. Lett.* **1994**, *224*, 24.
(28) Currie, G. N.; Ramsay, D. A. *Can. J. Phys.* **1971**, *49*, 317.
(29) Heldt, J.; Ottinger, Ch.; Vilesov, A. F.; Winkler, T. To be published.
(30) Spangler, L. H.; Pratt, D. W. *J. Chem. Phys.* **1986**, *84*, 4789.
(31) Spangler, L. H.; Pratt, D. W.; Birss, F. W. *J. Chem. Phys.* **1986**, *85*, 3229.
(32) Pebay Peyroula, E.; Jost, R. *J. Mol. Spectrosc.* **1987**, *121*, 177.
(33) Heldt, J.; Ottinger, Ch.; Vilesov, A. F.; Winkler, T. Book of Abstracts, The XVI. International Symposium on Molecular Beams, Ma'ale Hachamisha, Israel, 1995, p 5B.